

# Amphiphilic Heteroarm PEO-*b*-PS<sub>*m*</sub> Star Polymers at the Air–Water Interface: Aggregation and Surface Morphology

S. Peleshanko, J. Jeong, R. Gunawidjaja, and V. V. Tsukruk\*

Department of Materials Science and Engineering, Iowa State University, Ames, Iowa 50011

Received April 7, 2004; Revised Manuscript Received June 11, 2004

**ABSTRACT:** We report on the surface behavior of the asymmetric heteroarm poly(ethylene oxide) (PEO)/polystyrene (PS) star polymer on the air–water interface on a solid substrate. These amphiphilic star polymers with different numbers of hydrophobic arms and a similar hydrophilic block differ by architecture (four and three arm molecules, PEO-*b*-PS<sub>3</sub> and PEO-*b*-PS<sub>2</sub>), the length of PS chains (molecular weight from about 10 000 up to 24 000), and the number of PS arms (three and two). Detailed analysis revealed that well-developed circular domain surface morphology was formed at the air–water interface. Similar to linear diblock PEO–PS copolymers, the asymmetric heteroarm star polymers at low surface pressure formed circular nanoscale aggregates composed of PS arms. At higher surface pressure, the packing of circular domains became denser, but no clear transition to cylindrical structures was observed in condensed monolayers, contrary to linear block copolymers of similar composition. Therefore, we suggest that for star architecture the formation of highly curved interfaces is heavily favored, domain structure. This surface morphology remained stable even at very high compression close to the monolayer collapse unlike linear diblock copolymers with their tendency for structural reorganization even at very modest compressions.

## Introduction

Functionalized block copolymers are widely studied for their ability to form organized micellar aggregates with different morphologies in polymer solutions, bulk state, and in thin polymer films at surface and interfaces.<sup>1,2</sup> These studies have mainly focused on reporting synthesis of block copolymers and the microphase separation of these multicomponent copolymers in bulk<sup>3,4</sup> and sol–gel<sup>5</sup> states as well as aggregation properties in solution,<sup>6–8</sup> at interfaces,<sup>9,10</sup> and surfaces.<sup>11</sup> One of the most exploited diblock copolymers is non-ionic, poly(ethylene oxide) (PEO)–polystyrene (PS) diblock copolymer. The properties of these PEO–PS copolymers with variable molecular weight and chemical composition were widely studied in their bulk behavior,<sup>12</sup> phase structures,<sup>13</sup> and morphologies,<sup>14,15</sup> as well as their micellar structures in water<sup>16</sup> and organic solvents of different qualities.<sup>12,17–19</sup> Recent activities have focused on their ability to form stable monolayers at the air/water interface transferable to solid surfaces. The interfacial behavior and microstructure of PEO–PS block copolymers at both air–water and solid–air interfaces have been studied during the past few years by different research groups.<sup>20–30</sup>

Recent advances in polymerization have allowed the sophisticated synthesis of nontraditional block copolymers with complex macromolecular architectures extending beyond linear diblock copolymers such as grafted, star, and multiarmed copolymers, hyperbranched and dendritic polymers, dendrimer-like polymers, and star polymers with hyperbranched or dendritic fragments attached to the end of arms.<sup>31–33</sup> These systems are expected to be very peculiar in terms of their interfacial behavior and surface properties and differ significantly from linear block copolymers due to

constraints introduced by the chain attachment to a single center.<sup>34</sup> In the past years, a number of branched PEO–PS block and graft copolymers,<sup>35</sup> heteroarm (miktoarmed) copolymers,<sup>36</sup> multiarmed symmetrical copolymers,<sup>37–39</sup> and Gemini<sup>40</sup> and Janus-type<sup>41</sup> copolymers have been synthesized and studied. The miktoarm or heteroarm star polymers were a focus of recent studies.<sup>42,43</sup> It has been observed that the physical adsorption of miktoarm block copolymers on different substrates results in the selective collapse of one type of arms while concurrently inducing the extended state of arms of different types.<sup>44</sup> Francis et al. demonstrated the formation of dense hexagonally packed PS spheres from amphiphilic PEO<sub>3</sub>–PS<sub>3</sub> star block copolymer at the air–water interface (Langmuir monolayer) at low (<5 mN/m) surface pressure.<sup>39,43</sup> At higher surface pressures, the formation of PS rods surrounded by PEO regions followed with the monolayer collapse. Possible scenarios responsible for the restructuring of the monolayer includes initial spontaneous aggregation and changing conformation of the PEO chains due to their submergence in the water subphase during compression.

A lot of attention has been paid to star block copolymers with symmetrical architecture as with asymmetrical star architecture tested only on few occasions. On the other hand, all star block copolymers synthesized and studied to date possess “dead” terminal groups (e.g., methyl groups) which are not capable of further modification and chemical reactions such as grafting of these copolymers to solid substrates and at interfaces. This kind of interfacial design can be of interest for applications where shear stresses are concentrated along the interface.<sup>45–47</sup>

Here, we focus on the investigation of amphiphilic heteroarm PEO–PS star block copolymers of asymmetric type with a variable number of hydrophobic arms with different molecular weights. We report on the interfacial behavior at the air–water interface, surface

\* To whom correspondence should be addressed. E-mail: vladimir@iastate.edu.

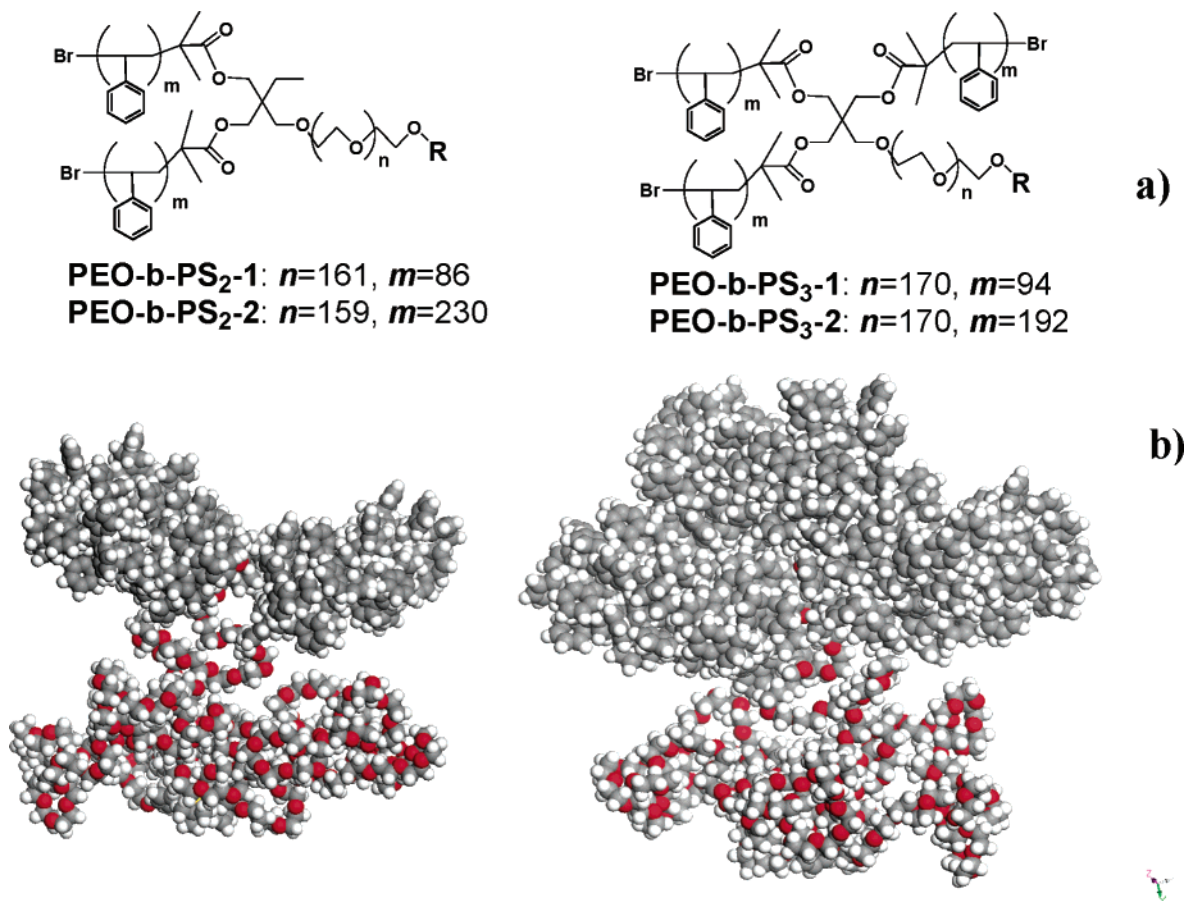


**Figure 1.** Chemical formulas of the star-block copolymers studied in this work with their corresponding abbreviations (a) and molecular models (b). Each model represents the low molecular weight specimens (b). R is the *tert*-butyldiphenylsilyl (*t*-Bu(Ph)<sub>2</sub>Si-) protecting group.

**Table 1. Properties of Star-Block Copolymers Used<sup>a</sup>**

polymer	GPC data total			NMR data							
	$M_n$ , 10 <sup>3</sup>	$M_w$ , 10 <sup>3</sup>	PDI	total $M_n$ , 10 <sup>3</sup>	PEO arm			wt	PS arm		$\epsilon$
					$M_n$ , 10 <sup>3</sup>	$N$	$j$		$M_n$ , 10 <sup>3</sup>	$N$	
PEO- <i>b</i> -PS <sub>3</sub> -1	23.3	27.0	1.16	37.0	7.5	170	0.18	0.20	9.8	94	4.6
PEO- <i>b</i> -PS <sub>3</sub> -2	38.2	45.6	1.19	67.0	7.5	170	0.10	0.11	20.0	192	4.3
PEO- <i>b</i> -PS <sub>2</sub> -1	19.2	24.8	1.29	25.0	7.1	161	0.26	0.27	8.9	86	3.0
PEO- <i>b</i> -PS <sub>2</sub> -2	47.4	54.8	1.18	54.8	7.1	159	0.11	0.13	23.9	230	2.8
PEO-PS-1	17.8	22.1	1.24	18.5	6.5	148	0.35	0.36	12.0	116	2.2
PEO-PS-2	35.4	42.4	1.19	38.1	17.3	394	0.43	0.45	20.4	196	1.5

<sup>a</sup>  $N$  is the degree of polymerization,  $\varphi$  is the volume fraction of PEO, wt is the weight fraction of PEO, and  $\epsilon$  is the asymmetry parameter.

morphology, and film microstructure on a solid substrate for two different amphiphilic heteroarm star copolymers with three and four arms (see chemical formulas in Figure 1a). We kept the same length of the hydrophilic block for all copolymers and changed the number and the length of the hydrophobic arms. Unlike the star block copolymers studied earlier, our copolymers represent the case of predominantly hydrophobic materials with the PEO block playing a role of a hydrophilic anchor. We expect that, under these conditions, crowding of the multiple PS chains in the vicinity of a junction point will affect the interfacial behavior and will heavily favor the formation of highly curved interfaces, thus, circular domain morphology. Comparative studies of block copolymers with one, two, and three PS arms of similar length will allow us to elucidate the role of branching. The synthesis of these star-block copolymers and their bulk structure are described in a separate publication.<sup>48</sup>

## Experimental Section

**Materials.** The amphiphilic heteroarm PEO-*b*-PS<sub>3</sub> and PEO-*b*-PS<sub>2</sub> star-block copolymers were synthesized by anionic polymerization of ethylene oxide followed by atom transfer radical polymerization (ATRP) of styrene as has been reported previously (Figure 1a).<sup>48</sup> These star-block copolymers have different numbers and lengths of PS chains and a relatively low polydispersity index as was confirmed by a combination of gel-permeation chromatography (GPC), nuclear magnetic resonance (NMR), and arm disassembling techniques (Table 1).

**Substrate Preparation.** The solid substrates were freshly cleaned, atomically smooth, [100] silicon wafers of high quality surface with microroughness not exceeding 0.1 nm within 1 × 1 μm<sup>2</sup> surface areas (Semiconductor Processing Co). These silicon wafers were cut in rectangular pieces of ~1 × 2 cm<sup>2</sup> and cleaned to remove any organic and inorganic contaminants from the surface according to the standard procedure.<sup>49</sup> Initially, silicon wafers submerged in Nanopure water ( $\sigma > 18.0$  MΩ cm) were treated for 10 min in an ultrasonic bath at

room temperature. Next, they were cleaned with a hot "piranha solution" (30% concentrated hydrogen peroxide, 70% concentrated sulfuric acid, *hazardous solution!*) for 1 h to remove organic contaminants and strip the original silicon oxide surface layer. Finally, the treated substrates were abundantly rinsed with Nanopure water and dried with a dry nitrogen stream. This treatment resulted in a fresh silicon oxide layer of very consistent thickness of about 1.2 nm with a high concentration of silanol groups. Wafer preparation was conducted in a clean room, class 100, to avoid any air contaminations on active surfaces.

**Sample Characterization.** The study of the surface behavior at the air–water interface and Langmuir–Blodgett (LB) monolayer deposition on to silicon substrate were conducted using an LB trough R&K 1. The 35–60  $\mu\text{L}$  of dilute polymer solution (concentration of 1 mg/L and lower) in chloroform (HPLC grade) was deposited dropwise (5–6 uniformly distributed locations) onto the Nanopure water surface and left to evaporate and spread for 30 min at 22 °C. The Langmuir monolayer formed was gradually compressed at the rate of 100  $\mu\text{m/s}$  to a specific pressure. The monolayer was held at this pressure to test its stability, and decompression–compression cycles were repeated to test the reversibility of the surface behavior. During the LB deposition, the surface pressure was held constant, as the submerged silicon substrate was slowly lifted from the trough. The LB monolayers were deposited onto the silicon substrates at different surface pressures ranging from very low (undistinguishable from zero line or "zero" pressure) to very high pressure on the verge of collapse. Two depositions at each specific pressure were performed for each polymer. The deposited LB monolayers were characterized with AFM after drying in a desiccator for 24 h.

The effective thickness of the deposited monolayers was measured with a COMPEL automatic ellipsometer (InOmTech, Inc.) with an incident angle of 70° and a wavelength of 634 nm according to the well-known experimental procedure.<sup>50a</sup> The average thickness of the silicon oxide layer was measured prior to the layers deposition and later used during the ellipsometry measurement where the double-layer model was employed to calculate the monolayer thickness. The refractive indexes used for the layers of amphiphilic copolymers were calculated by taking into account the chemical compositions of each copolymer. The refractive index values for different blocks were taken as 1.59 for PS and 1.53 for PEO.<sup>50b</sup> The results were averaged over five independent measurements at different locations on the substrate. The standard deviation of the thickness measured with ellipsometry was 0.1 nm.

The LB monolayers on the silicon substrates were studied with atomic force microscopy (AFM) by using Dimension-3000 and Multimode microscopes (both from Digital Instruments, Inc.) in the "light" tapping mode in accordance to the usual procedure adapted in our lab.<sup>51,52</sup> An amplitude ratio of 0.95 and higher was employed to avoid damaging the monolayers.<sup>53</sup> The scanning was conducted at 1 Hz for surface areas ranging from 20  $\times$  20  $\mu\text{m}^2$  to 500  $\times$  500  $\mu\text{m}^2$  and for several randomly selected locations with at least 40 different images collected for each specimen. The tip radius was measured independently using gold nanoparticles as a standard reference and only the sharpest tips were selected for scanning.<sup>54a</sup> The typical AFM tip radii were between 10 and 30 nm and the typical spring constants of these tips were in the range 40–60 N/m. The domain heights were obtained by cross-sectional analysis. The surface area coverage of domains was calculated from histogram using the bearing analysis.<sup>54b</sup> Both measurements were conducted with the assumption that domains were composed predominantly of PS phase.

Molecular models were built using Materials Studio 3.0. Energy minimization combined with cycles of molecular dynamics were used to build randomly coiled star polymers.

## Results and Discussions

**Behavior at the Air–Water Interface.** The star copolymers, PEO-*b*-PS<sub>2</sub> and PEO-*b*-PS<sub>3</sub>, studied here

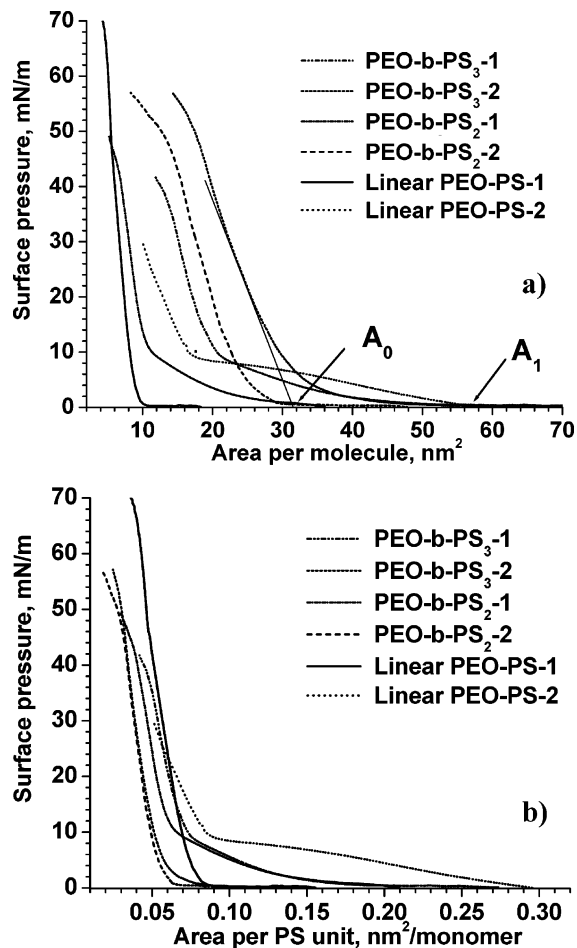


**Figure 2.** (a) Pressure–area isotherms for the Langmuir monolayers generated from the PEO–PS star–block and linear diblock copolymers. Each polymer is labeled according to their molecular weights as determined by NMR. (b) Compression isotherms normalized to the unit area of PS monomer.

possess the same length of the PEO arm and different lengths of the PS arms. For molecules with shorter PS chains (PEO-*b*-PS<sub>2</sub>-1 and PEO-*b*-PS<sub>3</sub>-1, Table 1), their overall size (as well as cross section) in random conformation is slightly smaller than that for PEO chains as is visualized by the molecular model (Figure 1b). In contrast, for molecules with longer PS chains (PEO-*b*-PS<sub>2</sub>-2 and PEO-*b*-PS<sub>3</sub>-2), PS chains form random coils with much larger overall dimensions, which completely overshadow the PEO chain (Figure 1b). Considering that a strong segregation of the dissimilar chains is expected at the air–water interface with PEO chains submerged in water and PS chains segregating above the water surface, such different ratios of geometrical dimensions should significantly affect their amphiphilic behavior as was initially revealed by pressure–area isotherms.

The general shape of the isotherms was a characteristic of classic amphiphilic behavior (Figure 2a).<sup>55</sup> All isotherms showed a steady increasing surface pressure upon compression and were reversible up to modest surface pressures. We did not observe any hysteresis of monolayers for the linear diblock PEO–PS-2 or for PEO-*b*-PS<sub>3</sub>-1 and PEO-*b*-PS<sub>2</sub>-1 at pressures below the formation of condensed monolayers. In addition, the monolayers were very stable under constant pressure, displaying virtually zero creep behavior at all pressures studied here.

The shape of the isotherms presented here is similar to the surface-pressure isotherms obtained for linear diblock PEO-PS copolymers with relatively low content of hydrophilic block.<sup>20,23,25</sup> The volume fraction for all the star polymers studied here is in the range from 10% to 26% (Table 1). A detectable (our balance sensitivity is about 0.2 mN/m) increase of the surface pressure was observed for areas per molecule below 40–60 nm<sup>2</sup>, with a sharp rise in the surface pressure observed for the surface areas below 20 nm<sup>2</sup> indicating the formation of the condensed monolayer state above 10 mN/m (Figure 2a). A very long range of virtually constant, close to zero, surface pressure was observed for star copolymers at low compressions. The isotherms for PEO-*b*-PS<sub>3</sub>-1 and PEO-*b*-PS<sub>2</sub>-1 showed some evidence of the pseudo-plateau. However, due to the extremely low surface pressures it is not easy to confirm its presence directly. This can be an indication of the corresponding intralayer transformation usually observed for traditional block copolymers with higher PEO content described in the literature.<sup>20,25,27</sup> In contrast, for PEO-*b*-PS<sub>3</sub>-2 and PEO-*b*-PS<sub>2</sub>-2 star polymers, we did not observe any pseudo-plateau on the isotherms due to a low PEO content. All pressure–area isotherms for star–block copolymers were consistently shifted to higher surface areas with increasing molecular weight of the PS arms (Figure 2a). Linear PEO-PS block copolymers with different PEO content showed behavior similar to that reported in the literature.<sup>26</sup> The isotherm shape for this linear block copolymer is a signature of PEO-PS amphiphilic copolymers with sufficient amount of PEO block.<sup>21,28</sup> Normalization to a PS monomeric unit showed significant difference in the isotherms of linear block copolymers with different PEO block content indicating controlling role of this block in surface behavior (Figure 2b). On the other hand, isotherms for star block copolymers with different molecular weights of the PS blocks showed minor differences indicating similarity of the surface structures. The increase in the number of PS arms from two to three resulted in a shift of the normalized isotherms to the large area, pointing to a more spread state of PS arms in the latter case.

For diblock PEO-PS copolymers, it was shown that at low surface density the hydrophobic PS block collapsed in insoluble, mainly spherical, domains, while the hydrophilic PEO block adopted a flattened state with most of the PEO segments forming water complexes and coming in contact with the water surface. It was suggested that this regime is characterized by the pancakelike structure of PEO block with numerous specific features to be offered for different amphiphilic block copolymers and for the surface areas per molecule in the range of the so-called plateau region (see the isotherm for the linear diblock copolymer with higher PEO content in Figure 2a).<sup>20,56,27,28</sup>

The surface area per molecule,  $A_0$ , for all of the monolayers was calculated by extrapolating the steep rise in the surface pressure back to the zero level of the LB isotherms was in the range 11–24 nm<sup>2</sup> (Table 2).<sup>57</sup>  $A_1$  is the surface area per molecule at the lowest distinguishable (<0.2 mN/m) surface pressure, which corresponds to the initial formation of a loosely packed monolayer. The numerical values of  $A_0$ , indicating the onset of a condensed monolayer formation, differed significantly for the different star–block copolymers with increasing values observed for the copolymers with higher molecular weight of the hydrophobic PS arms

**Table 2. Calculated Dimensions of PS Chains and Observed Surface Areas of the Heteroarm Star Polymers<sup>a</sup>**

polymer	random coiled PS chain			collapsed PS phase	experiment	
	$R_0$ , nm	$A_0/\text{arm}$ , nm <sup>2</sup>	$A_0/\text{total}$ , nm <sup>2</sup>	$A_0/\text{total}$ , nm <sup>2</sup>	$A_0$ , nm <sup>2</sup>	$A_0/\text{PS unit}$ , nm <sup>2</sup>
PEO- <i>b</i> -PS <sub>3</sub> -1	3.03	28.7	86.2	16.8	21	0.074
PEO- <i>b</i> -PS <sub>3</sub> -2	4.64	67.7	203.3	27.2	31	0.054
PEO- <i>b</i> -PS <sub>2</sub> -1	2.87	25.8	77.5	13.2	11	0.064
PEO- <i>b</i> -PS <sub>2</sub> -2	5.18	84.1	252.5	23.4	24	0.052
PEO-PS-1	3.56	39.8	39.8	10.8	8.2	0.071
PEO-PS-2	5.14	83	83	15.0	19.0	0.097

<sup>a</sup>  $R_0$  is the radius of gyration of PS chains in a random coil conformation;  $A_0/\text{arm}$  is the surface area per arm,  $A_0/\text{total}$  is the surface area of all PS blocks,  $A_0/\text{PS unit}$  is the surface area per PS unit.

(Figure 2a, Table 2). It is expected that at higher surface pressure, the PEO block will be completely submerged in the water subphase with the steric repulsion between PS blocks becoming the dominating factor in the formation of the condensed monolayer.

The effective thickness of Langmuir monolayers transferred on the solid substrate was measured at a series of surface pressures in the range 0–25 mN/m (Figure 3a). The effective thickness increased from 0.3 nm for “zero” pressure to 5 nm for the star–block copolymers at the highest pressure. The increase of the monolayer thickness was consistent for all of the star polymers with a systematic shift to higher values for the molecules with higher molecular weight of PS arms. Correspondingly, the surface area per molecule measured independently from the isotherms was gradually decreasing with increasing of the surface pressure thus keeping the overall volume per molecule fairly unchanged except at extremely low surface pressures (Figure 3b).

The area per molecule in the compressed monolayer state vs the total molecular weight of PS arms for all four star–block copolymers with two and three arms studied here is presented in Figure 3c. These data, although very limited in the range covered, can be approximated by a power function with the exponent value of  $0.76 \pm 0.15$  that is close but higher than the expected  $2/3$  value for a simple unconstrained increase of the molecular volume of spherical domains without changing conformation and density of the molecular packing. This result, although supported by limited statistics, is indicative of the trend seen for extended state of the lengthening hydrophobic arms attached to the single joint, unlike the usual random coil expansion observed for linear diblock copolymers. This behavior is expected because of crowding of the PS arms near the star junction point as predicted in the literature.<sup>58</sup> In fact, this behavior was observed for miktoarm PS-PI star copolymers in bulk state where the long period increases with increasing number of PS arms.<sup>59</sup> This and other trends discussed below can be related to space constraints imposed by a common joint point of a conformation of the arms in condensed state. Indeed, the estimation of the surface area per PS monomer unit resulted in the values within 0.05–0.07 nm<sup>2</sup>/unit for star polymers (Figure 2b) as compared to the usual value of about 0.08–0.1 nm<sup>2</sup>/unit for linear diblock copolymers and for a linear copolymer studied in this work (Table 2). Considering that the surface areas per PS monomeric unit in star–block copolymers were

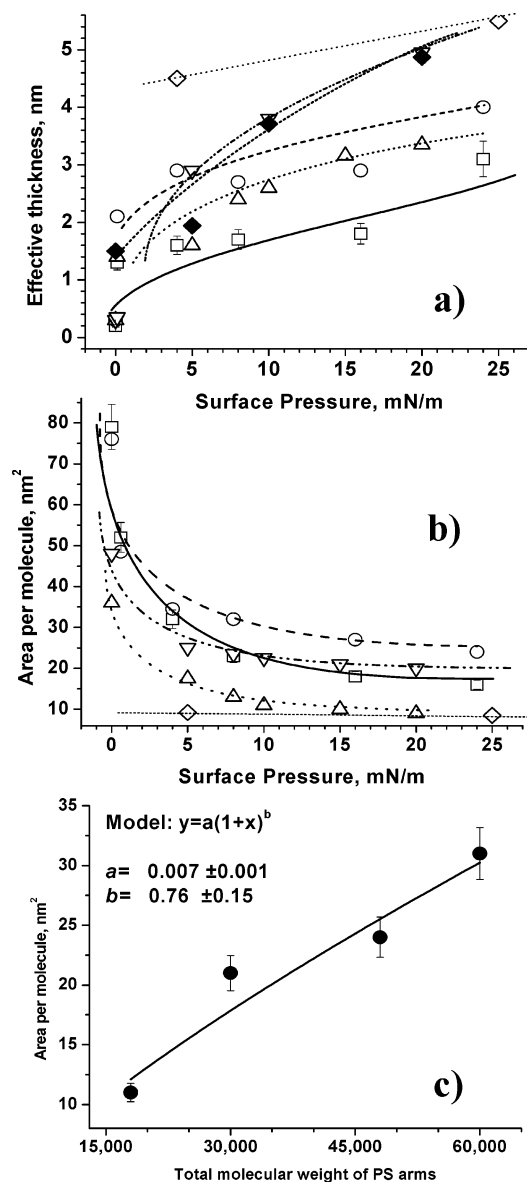


**Figure 3.** (a) Variations in the effective thickness of the monolayer, (b) the surface area per molecule of the star–block and linear diblock copolymers vs surface pressure, and (c) variations in the surface area per molecule of the star–block copolymers as a function of total molecular weight of PS arms, as determined from their Langmuir–Blodgett monolayers and Langmuir isotherms, respectively: PEO-*b*-PS<sub>3</sub>-1 (□); PEO-*b*-PS<sub>3</sub>-2 (○); PEO-*b*-PS<sub>2</sub>-1 (△); PEO-*b*-PS<sub>2</sub>-2 (▽); linear diblocks PEO–PS-1 (◇) and PEO–PS-2 (◆). All lines are drawn as guides for the eye.

significantly lower than that for the linear block copolymer, we can conclude that multiple PS chains connected to a single joint are more packed than in linear copolymers.<sup>40</sup>

Additional insight into the polymer chain conformation can be obtained by comparing their dimensions and the experimentally obtained surface area per molecule.<sup>21</sup> We calculated the expected surface areas for both arms assuming either their unperturbed conformation or completely collapsed state and compared these values to the experimental ones obtained from the pressure–area isotherms for the limiting area of the formation of the condensed monolayer ( $A_0$ ) and the initial stage of the formation of loosely packed monolayer ( $A_1$ ) (Figure 2a). The radius of gyration  $R_0$  for both PS

**Table 3.** Calculated Dimensions of PEO Chains and Observed Surface Areas of the Heteroarm Star Polymers<sup>a</sup>

polymer	theoretical		experimental	
	$R_0$ , nm	$A_1$ , nm <sup>2</sup>	$A_1$ , nm <sup>2</sup>	$A_1$ /PEO unit, nm <sup>2</sup>
PEO- <i>b</i> -PS <sub>3</sub> -1	4.52	64.16	56	0.33
PEO- <i>b</i> -PS <sub>3</sub> -2	4.52	64.16	48	0.28
PEO- <i>b</i> -PS <sub>2</sub> -1	4.34	60.11	36	0.23
PEO- <i>b</i> -PS <sub>2</sub> -2	4.34	59.21	48	0.30
PEO–PS-1	4.02	50.77	12	0.08
PEO–PS-2	6.61	132.26	57	0.15

<sup>a</sup>  $R_0$  is the radius of gyration of PEO chain in a random coil conformation.  $A_1$  is the total surface area of PEO chain,  $A_1$ /PEO unit is the surface area per PEO unit.

and PEO chains in a random coil conformation was calculated according to<sup>60,61</sup>

$$R_0 = \sqrt{\frac{aN^{3/5}}{6}} \quad (1)$$

where  $a$  is the segment length (Kuhn segment) and  $N$  is the number of segments (Tables 2 and 3). The number of segments  $N$  is calculated according to following equation:

$$N = N_t/n_s \quad (2)$$

Here  $n_s$  is the number of monomer units in one Kuhn segment, and  $N_t$  is the number of monomer units in the polymer chain. The literature data used for the two blocks are as follows: for PS,  $a = 1.69$  nm and  $n_s = 6$ ; for PEO,  $a = 0.77$  nm and  $n_s = 2$ .<sup>62</sup> The molecular volumes of PS and PEO chains were calculated from known molar values for the bulk state,<sup>63,64</sup> and the corresponding occupied areas were calculated assuming a spherical shape at the air–water interface.

The comparison of chain dimensions with the limiting surface area per molecule in the condensed state shows that the experimental area per molecule in condensed state was much lower than that calculated for the undisturbed PS chains (Table 2). However, these values are reasonably close (within  $\pm 20\%$ ) to the areas per molecule calculated from the molecular volume of the collapsed PS chains (Table 2). The collapsed state of the hydrophobic blocks of amphiphilic block copolymers exposed to the air was expected.<sup>65</sup> This is a clear confirmation of the predominant role of the PS chains in the formation of the condensed monolayer of star–block copolymers as is widely recognized for linear block copolymers.<sup>22</sup> It is also confirmed by computational modeling of the star polymers (Figure 1b).

The observed dimensions of the PEO chains remain virtually unchanged for all star–block copolymers due to similar molecular weight (Table 3). It is clear from this evaluation that the PEO chains in undisturbed conformation should occupy much larger surface area than that observed experimentally for the condensed monolayers. On the other hand, this area was fairly close to that observed for the onset of the initial stages of the formation of the loose monolayer (Table 3). Moreover, the calculated surface area per PEO unit for all star–block copolymers is within 0.23–0.33 nm<sup>2</sup>, which is close to the surface area estimated for the PEO monomeric units oriented at the water surface and hydrogen-bonded with 1–3 molecules of water (0.28 nm<sup>2</sup> for the PEO monomeric unit with two water mol-

ecules).<sup>22,24,66</sup> Thus, we suggest that for the star–block copolymers studied here the onset of the formation of the monolayer at the air–water interface is determined by the initial interaction of the hydrated PEO chains spread at the water surface around collapsed PS domains similar to conventional linear block copolymers. Accordingly, in the condensed monolayer state, the PEO chains should become desorbed from the air–water interface and stretched in the vertical dimension to adopt the brush conformation controlled by the diminishing surface area from the compression of PS domains as was suggested for conventional linear block copolymers.<sup>29</sup>

**Morphology of Langmuir–Blodgett (LB) Monolayers at the Solid–Air Interface.** Langmuir–Blodgett transfer of these monolayers onto a solid substrate allows a detailed characterization of their morphology. It has been demonstrated that the morphology of amphiphilic organic materials in their monolayer state is usually preserved during this transfer under the optimal transfer conditions; thus, a close similarity between Langmuir and LB monolayers is usually postulated.<sup>67</sup> However, comparison of the PS domain heights and the overall thickness of the monolayer showed the thickness of the PEO phase in condensed monolayers varying from 0.6 to 1.7 nm depending upon the surface pressure and the types of polymer. Considering that the diameter of coiled PEO chains is close to 9 nm, we can conclude that the hydrophilic chains facing the hydrophilic surface after transfer to a solid substrate are spread very thin beneath the hydrophobic domains, covering the vast majority of the surface area. The number of star molecules within these domains was estimated to be within several hundred for low molecular weight star–block copolymers but increased to 1000–2000 for higher molecular weight star–block copolymers. For two linear PS–PEO block copolymers studied here (Table 1), we observed circular (dot) surface morphology at low surface pressure, which can be transformed to cylindrical morphology at higher pressures (not shown). However, the PEO content is systematically higher in these linear analogues despite the fact that the length of the PEO block in PEO–PS-1 is similar to that of the star block copolymers.

**Morphology of LB Monolayers at “Zero” Surface Pressure.** The AFM images of the LB monolayers transferred onto the solid substrate were used to study their morphology at a series of surface pressures representing the different stages of the monolayer formation during compression at the air–water interface. Considering that even modest monolayer compression results in instantaneous segregation of hydrophilic and hydrophobic blocks in block copolymers we paid a special attention to finding the “pre-segregated” or the “gas” state by adjusting the amount of the material deposited at the air–water interface (surface area available for molecule spreading) and lowering surface pressure below any detectable level (so-called “zero” pressure). Sheiko et al.<sup>68</sup> and Lord et al.<sup>69</sup> deposited monolayers of brush molecules on a solid substrate using LB technique at different surface pressure including the “gas” state, seeing individual molecules with a large spacing between them. Individual domains from fatty acids not forming continuous monolayers have been also deposited on a solid substrate in the “gas” state.<sup>70</sup>

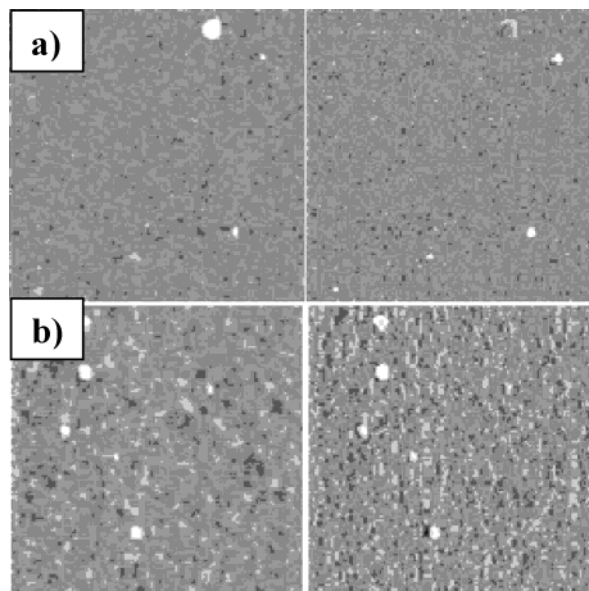


**Figure 4.** AFM images of the LB monolayers of amphiphilic heteroarm star PEO-*b*-PS<sub>3</sub>-1 (a) and PEO-*b*-PS<sub>3</sub>-2 (b) polymers deposited at 0 mN/m surface pressure (topography (left) and phase (right)). Scan size: (a)  $1 \times 1 \mu\text{m}^2$ , height scale is 3 nm, and phase scale is  $10^\circ$ ; (b)  $1 \times 1 \mu\text{m}^2$ , height scale is 10 nm, and phase scale is  $20^\circ$ .

For both three- and four-arm star polymers with different molecular weights, we succeeded in transferring a very thin monolayer without clear detectable segregated domain structure (see examples of surface morphologies in Figure 4). In this state, the monolayer looks uniform with very minor variations of topography and a low effective thickness close to 0.3 nm and microroughness below 0.4 nm. No signs of well-defined domain morphology are observed at this stage at high resolution, although a random network of surface corrugations on a scale of below 50 nm can be seen in both topographical and phase images. Further treatment of these surfaces with a bad solvent for PS block (water) results in significant surface roughening and the appearance of poor-defined random morphology with the height of the elevated areas about 1 nm. Thus, we conclude that under the conditions where a loose packing and exceeding surface are available for star molecules, they spread over the surface forming a surface layer in a “gas” state. However, this state of the spread molecules is spontaneously converted into the segregated state with heterogeneous domain morphology under very minute compression that probably explains the widespread belief that amphiphilic block copolymers of this type always spontaneously segregate at the air–water interface.<sup>24,26</sup>

**Morphology of LB Monolayers from Four-Arm Molecules in the Segregated State.** As was mentioned above, a very slight increase of the surface pressure beyond the lowest detectable limit (typically to 0.3–0.7 mN/m) result in the formation of highly segregated domain morphology. The domain morphology is consistently observed when the area per molecule decreases to about  $50 \text{ nm}^2$  (Figure 2a and Table 3). This compression results in the formation of a well-developed morphology with circular domains (see representative images in Figures 5–8).

At relatively low surface pressures, PEO-*b*-PS<sub>3</sub>-1 copolymer with a lower molecular weight of the PS arms forms small circular domains with uniform dimensions.

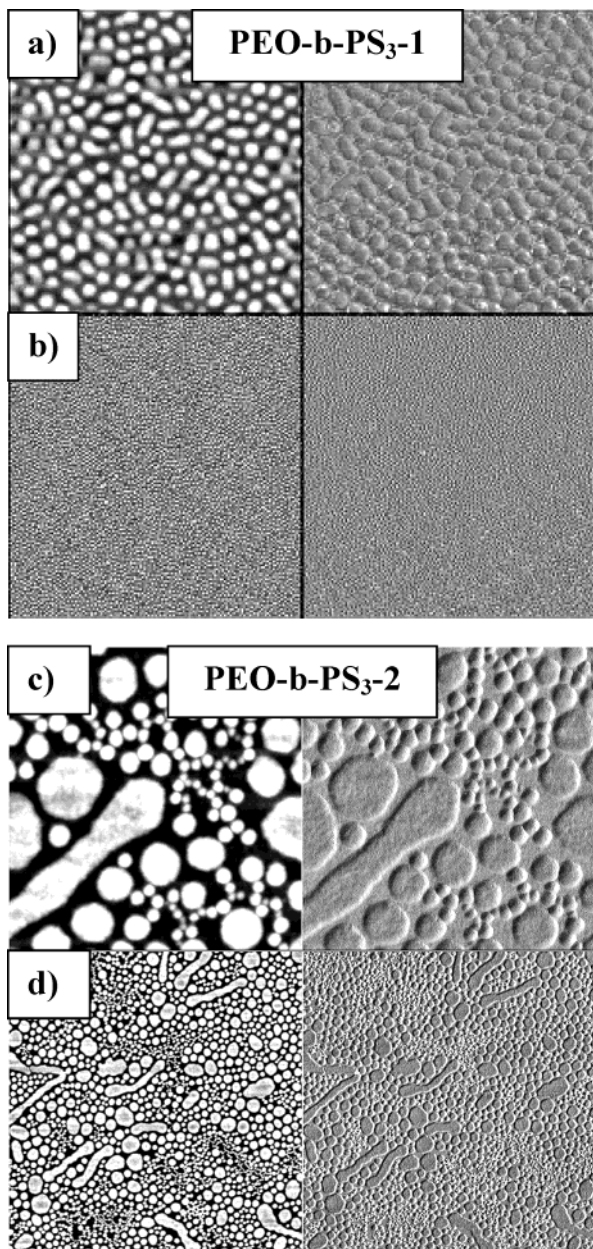


**Figure 5.** AFM images of the LB monolayers of amphiphilic heteroarm star PEO-*b*-PS<sub>3-1</sub> and PEO-*b*-PS<sub>3-2</sub> polymers deposited at 0.7 mN/m surface pressure (topography (left) and phase (right)). Scan size: (a and c)  $1 \times 1 \mu\text{m}^2$ , height scale is 5 nm, and phase scale is  $10^\circ$ ; (b and d)  $5 \times 5 \mu\text{m}^2$ , height scale is 15 nm, and phase scale is  $25^\circ$ .

In the same pressure range, PEO-*b*-PS<sub>3-2</sub> star copolymer with higher molecular weight forms predominantly circular domains with widely variable lateral dimensions due to partial coalescence (Figure 5). The effective thickness of the monolayer reaches 1.5 nm for PEO-*b*-PS<sub>3-1</sub> with the height of individual domains close to 3 nm (Figure 9). For the four-arm star polymer with higher molecular weight of PS arms the thickness increases even higher, to 2.5 nm, and the height of the individual domains approaches 6 nm. The predominant structural elements at all surface pressures are round, relatively uniform circular two-dimensional micelles with diameters ranging from 40 to 150 nm with occasional diameters of coalesced domains reaching 500 nm. The modest compression of the monolayer results in increasing packing density of circular domains to above 50% and their heights to 2–6 nm without

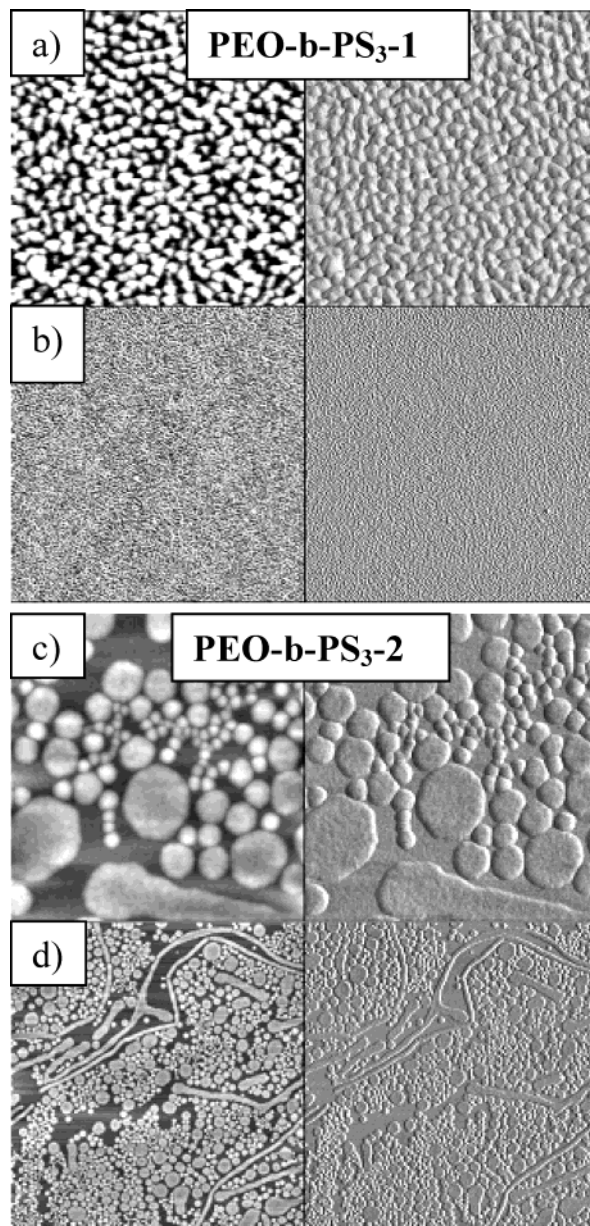


**Figure 6.** AFM images of the LB monolayers of amphiphilic heteroarm star PEO-*b*-PS<sub>3-1</sub> and PEO-*b*-PS<sub>3-2</sub> polymers deposited at 10 mN/m surface pressure (topography (left) and phase (right)). Scan size: (a and c)  $1 \times 1 \mu\text{m}^2$ , height scale is 5 nm, and phase scale is  $15^\circ$ ; (b and d)  $5 \times 5 \mu\text{m}^2$ , height scale is 10 nm, and phase scale is  $10^\circ$ .

significant changes in their lateral dimensions (Figures 5, 6 and 9).

It is worth noting, that all images presented here were collected far from the edges of the substrate to avoid additional influence caused by water flow, the meniscus, and the drying front on the monolayer morphology. As is known, for relatively stiff monolayers the surface morphology is uniform across the whole surface area including those located at the edges. However, for compliant polymer monolayers these contributions can, to a great extent, affect the alignment and the appearance of the domain structure causing such widely observed phenomena as texturing, biphasic morphology, wrinkles, and foldings.<sup>67,71</sup> Thus, we tested the uniformity of the surface morphology observed and its consistency over the whole surface area beyond the central portion of the substrate. As can be seen from several representative images collected along the sub-

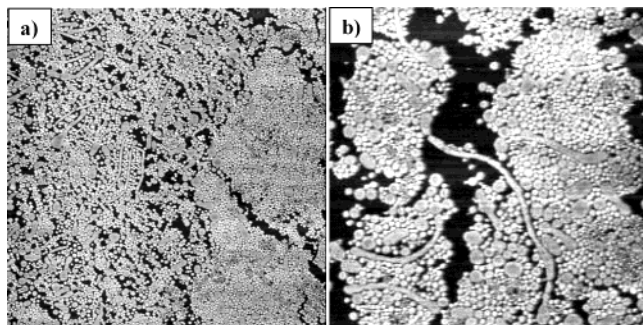


**Figure 7.** Topography images of the LB monolayers of amphiphilic heteroarm star PEO-*b*-PS<sub>3</sub>-2 deposited at 20 (a) and 30 mN/m (b) surface pressure. Scan size: 20 × 20 μm<sup>2</sup> (a) and 10 × 10 μm<sup>2</sup> (b), height scale is 10 nm.

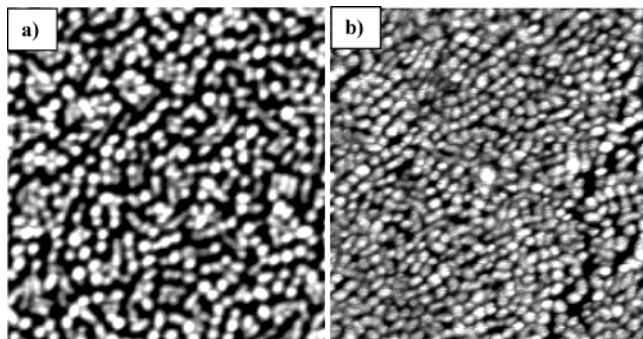


**Figure 8.** Topography images of the LB monolayers of amphiphilic heteroarm star PEO-*b*-PS<sub>3</sub>-1 deposited at 20 (a) and 30 mN/m surface pressure (b). Scan size is 2 × 2 μm<sup>2</sup>; height scales are 5 nm and 10 nm, respectively.

strate edges (Figure 10), a complex texture of highly oriented lamellar structures, coexistent biphasic regions, superimposed circular and multilamellar structures, and quasi-rectangular shaped domains all can be found along the edges of the substrates and along the contact line. The appearance of these morphologies is controlled by local transfer/flow/drying conditions within the selected surface areas.<sup>27b</sup> These possible contributions should be carefully taken into account in the course of the analysis of the surface morphology of these very mobile and compliant monolayers. These perturbances can be avoided to a great degree by lowering the transfer speed and conducting scanning far from the substrate edges.<sup>72</sup>

The increase of surface pressure above 10 mN/m leads to the formation of the condensed monolayers with the PS chains well separated and stretched out of interface. Correspondingly, a minor increase of the domain heights accompanied by the gradual but slow increase of the surface coverage was observed (Figure 9). The surface coverage with circular domains estimated from the AFM images with the correction for tip dilation (when measurements were technically possible) increased gradually to 60–70%. This constituted the highest possible limit of 2D packing of circular domains leaving very limited “free surface”.<sup>73</sup> In some surface areas for the PEO-*b*-PS<sub>3</sub>-2 copolymer, a partial coalescence of small circular domains into large dense circular areas of several hundred nanometers across was observed with smaller domains still preserving their identity within these areas (Figures 5, 6 and 7). The highest surface coverage was observed for the four-arm star polymer with higher molecular weight, PEO-*b*-PS<sub>3</sub>-2 (Figure 7).

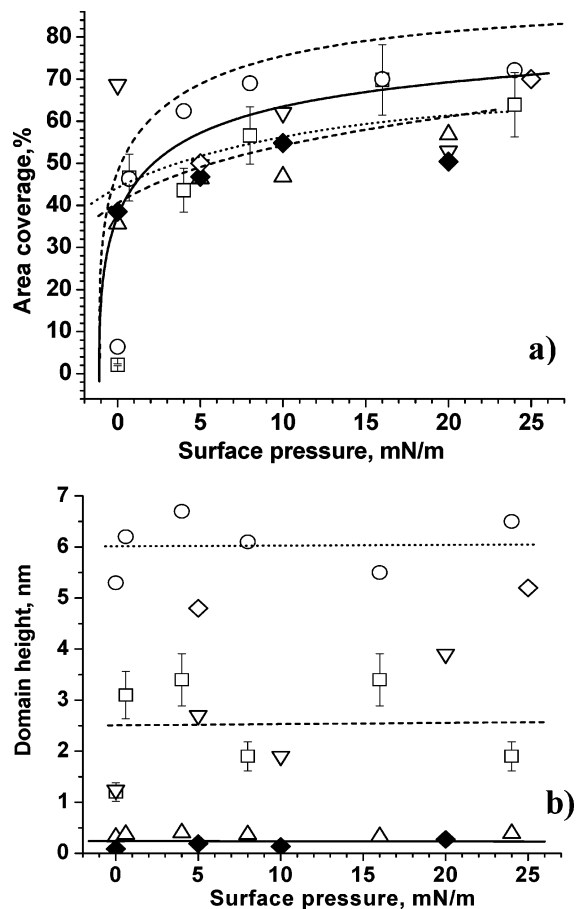


**Figure 9.** Variations in the surface area coverage (a) and heights (b) as a function of the surface pressure: PEO-*b*-PS<sub>3</sub>-1 (□); PEO-*b*-PS<sub>3</sub>-2 (○); PEO-*b*-PS<sub>2</sub>-1 (△); PEO-*b*-PS<sub>2</sub>-2 (▽); linear diblocks PEO-PS-1 (◇) and PEO-PS-2 (◆). All lines are drawn as guides for the eye.

### Morphology of LB Monolayers from Three-Arm Star Molecules in the Segregated State.

The surface morphology was also studied for the three-arm star polymers with different molecular weights of the PS arms (Figures 11). At low surface pressure barely exceeding the lowest limit of detection, the low molar weight three-arm polymer PEO-*b*-PS<sub>2</sub>-1 showed a well-developed circular domain morphology with very uniform heights of 1–2 nm and lateral dimensions of 30–50 nm. Lateral dimensions increased for PEO-*b*-PS<sub>2</sub>-2 with higher molecular weight reaching 40–70 nm at low surface pressure (Figures 5 and 6). The domains showed a large variability in lateral dimensions. General trends in variation of the monolayer thickness, domain heights, and surface coverage for this three-arm star-block copolymer followed that discussed for four-arm star polymers, as can be seen in the summary plots (Figures 3 and 9). Apparently, all parameters of surface morphology correlate well with the overall molecular weight of the PS blocks. However, one noticeable exception is the transformation of the surface morphology of three-arm block copolymer with low molecular weight from circular to cylindrical domain structure at elevated surface pressure, on the onset of the formation of the condensed monolayer.

### General Discussion

The theoretical consideration of the role of the asymmetrical architectures of diblock copolymers on the bulk

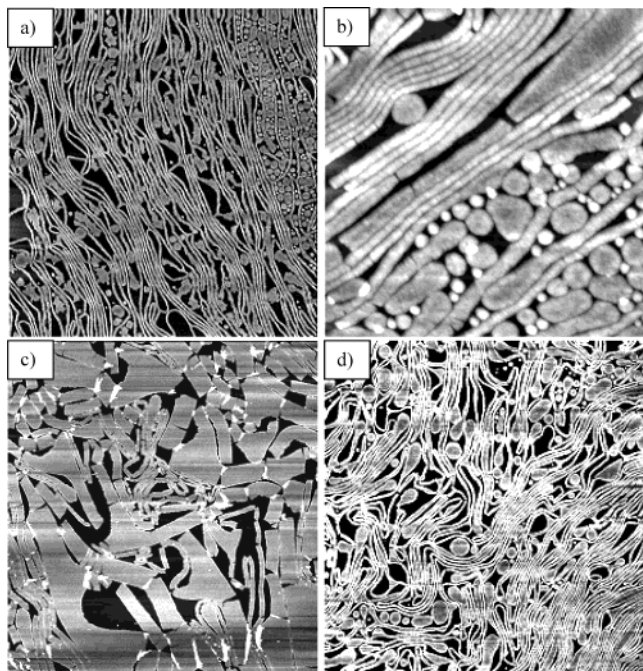


**Figure 10.** Topography images of the LB monolayers of amphiphilic heteroarm star PEO-*b*-PS<sub>3-2</sub> scanned at different locations along the edges and the contact lines of the silicon wafer: (a) at 5 mN/m surface pressure, the scan size is  $10 \times 10 \mu\text{m}^2$  and height scales are 10 nm; (b) at 30 mN/m surface pressure, the scan size is  $2 \times 2 \mu\text{m}^2$  and height scales are 15 nm. (c and d): Heteroarm star PEO-*b*-PS<sub>2-2</sub> deposited at 10 mN/m surface pressure, the scan size is  $20 \times 20 \mu\text{m}^2$  (c) with 10 nm height scale, and  $10 \times 10 \mu\text{m}^2$  (d), where the height scale is 5 nm.

microstructure showed that the presence of the multiple arms of one type causes their stretching away from the interface and curving of the interface.<sup>74</sup> This resulted in the effective shift of the boundary lines separating different morphologies on a phase diagram expressed in terms of the asymmetry parameter,  $\epsilon$ , and the volume fraction (Figure 12):<sup>75</sup>

$$\epsilon = (N_A/N_B) (V_A R_B^2 / V_B R_A^2)^{1/2} \quad (3)$$

where  $N$ ,  $V$ , and  $R$  are the number, the volume, and the end-to-end distance of A or B arms, respectively. This theory predicts that adding new arms while keeping the overall composition unchanged should result in transformation from lamellar  $\rightarrow$  cylindrical  $\rightarrow$  spherical morphology due to the stabilization of a more curved interface in the presence of the one-sided multiple arms. Such trends, although not confirmed quantitatively, are generally observed for the solid state of star-block copolymers.<sup>76</sup>

We suggest that the star-block copolymers considered in this paper follow the same trend predicted for the bulk state of asymmetrical star-block copolymers because the general conditions for packing of different blocks in two-dimensional states are similar to that existing in three-dimensional cases.<sup>77</sup> Under this assumption, we estimated the asymmetry parameter for star-block copolymers studied here and observed that their values are deeply "buried" in spherical (circular for two-dimensional state) shape territory far from the border between spherical and cylindrical morphologies (Figure 12). This is unlike linear diblock copolymers with identical chemical composition, which are close to the borderline between spherical and cylindrical struc-

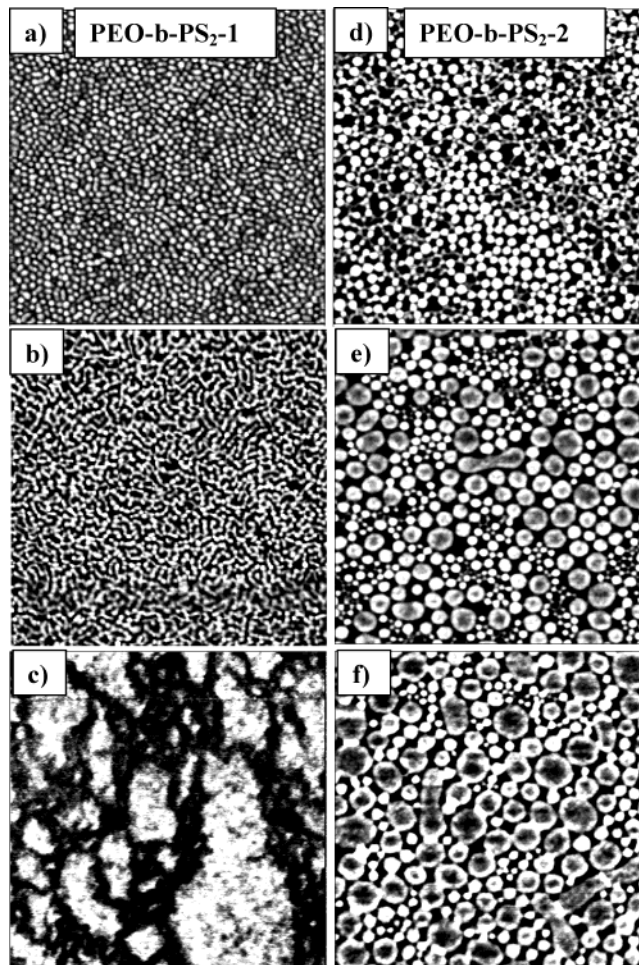


**Figure 11.** Topography images of the LB monolayers of amphiphilic heteroarm star PEO-*b*-PS<sub>2-1</sub> (a–c) and PEO-*b*-PS<sub>2-2</sub> (d–f) polymers deposited at the following surface pressures: 5 (a and d), 10 (b and e), and 20 mN/m (c and f). The scan size is  $2 \times 2 \mu\text{m}^2$ ; the height scale is 5 nm.

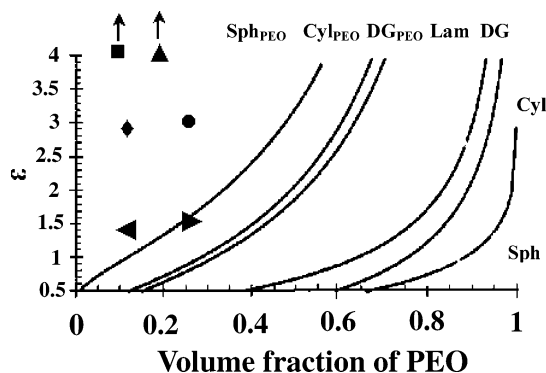


**Figure 12.** Top: Milner's phase diagram for the morphologies of  $A_n-B_m$  asymmetrical block copolymers adapted from that reported in the literature.<sup>75</sup> The asymmetrical parameters calculated for the linear and heteroarm star PEO-PS block copolymers are represented as follows: PEO-*b*-PS<sub>3-1</sub> ( $\blacktriangle$ ); PEO-*b*-PS<sub>3-2</sub> ( $\blacksquare$ ); PEO-*b*-PS<sub>2-1</sub> ( $\bullet$ ); PEO-*b*-PS<sub>2-2</sub> ( $\blacklozenge$ ); hypothetical linear diblock PEO-PS copolymers with the same composition as the PEO-*b*-PS<sub>2-1</sub> (solid triangle right) and PEO-*b*-PS<sub>2-2</sub> (solid triangle left).

tures (Figure 12). Thus, a linear architecture for similar block copolymers would favor less curved interfaces making them more prone to the transformation from initial circular shape to cylindrical morphology during compression. The presence of the air-water interface and the segregation of PS chains across this interface

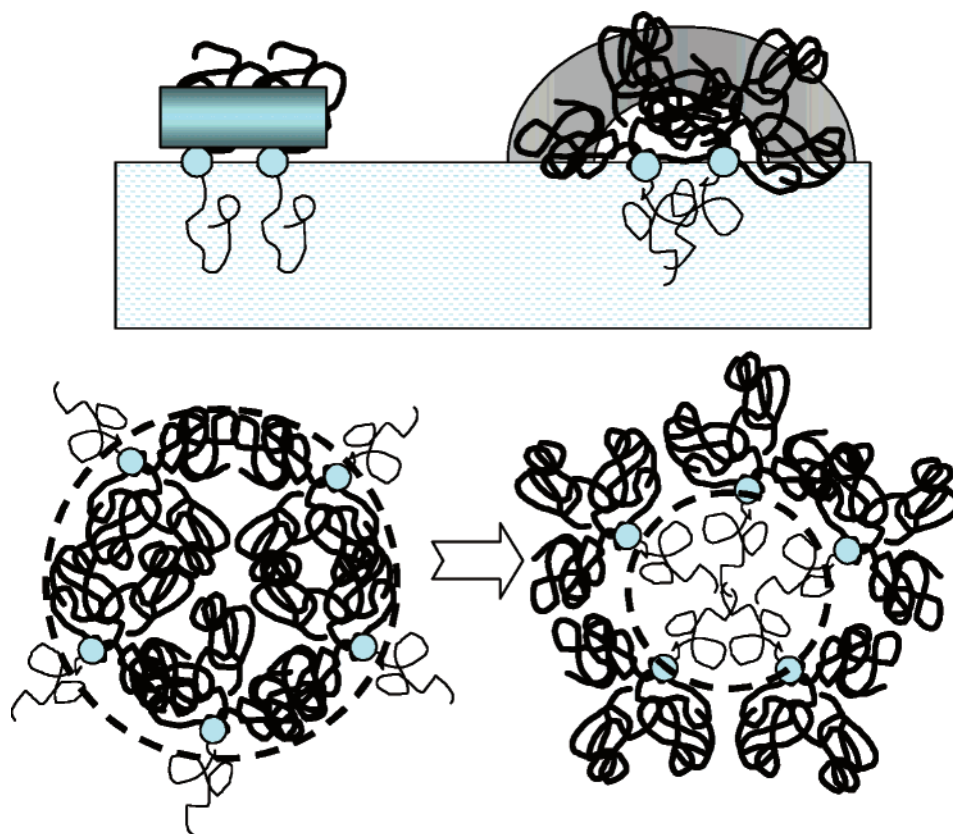


**Figure 13.** Top: schematics of the chain behavior for linear diblock copolymer (left) and star block copolymer (right) at the air–water interface (side view). Bottom: corresponding top view of less-favorable circular domain structure (left) and more favorable inverse circular domain structure with PEO chains surrounded by PS phase (right).

complicates the situation. Segregation across the interface favors strongly curved, convex shapes of PS domains as illustrated in Figure 13. However, in-plane segregation of PS chains and surface-anchored PEO chains makes two-dimensional circular shape less stable providing conditions for inverse circular micelle formation (Figure 13). The overall balance of these different trends could result in a variety of interfacial scenarios different from those expected for diblock copolymers.

The details of the monolayer microstructure of PS–PEO block copolymers depend strongly upon the fabrication conditions, chemical architecture, and chemical composition as debated in a number of recent publications.<sup>27,29,72</sup> Although, it is clear that the general trend in the formation of the interfacial morphology for star–block copolymers studied here is similar to that reported before for conventional linear block copolymers, here we will discuss several distinguished features which we believe could be attributed to the peculiar architecture of these star-shaped molecules. Several recent studies dealing with PS–PEO copolymers with a composition similar to that studied in this paper are relevant for this discussion.

A different star architecture but with molecular weight and chemical composition similar to the star polymers studied here was considered by Francis et al.<sup>43</sup> The authors showed that initially formed hexagonal pattern of the PEO<sub>3</sub>-*b*-PS<sub>3</sub> star copolymer with  $M_n = 30\,000$  and wt of PEO, around 20% changed to rod like structure upon compression at surface pressure around 5 mN/m. Further increase of the surface pressure led to denser packing of newly formed rodlike domains with final collapse of the monolayer around 30 mN/m.

Baker and Devereaux using linear PEO–PS block copolymers with total molecular weight between 200 000 and 375 000 (wt PEO between 15% and 92%)<sup>27</sup> showed that PEO–PS block copolymers with greater than 10% PEO formed only dotlike domains with small size and spacing which was controlled by deposition pressure. However, very high molecular weights of these block copolymers (10 times higher than for those studied in our work) suggested stronger segregation behavior than that characteristic for our block copolymers. For a copolymer with a slightly lower molecular weight that was closer to that of our compounds (total molecular weight of 51 300 and PEO weight fraction of 7%)<sup>27b</sup> several different types of surface structures including dots, spaghetti, and rodlike micelles were observed as a result of different spreading concentrations and deposition conditions. All films were deposited at relatively low surface pressures between 0.3 and 10 mN/m. At a surface pressure of 10 mN/m, a phase transition occurred as the PEO chains begin to form brushes. However, no results were discussed on the film morphology at surface pressures higher than 10 mN/m.

Several linear PEO–PS block copolymers which can be directly compared with our star copolymers have been studied by Cox et al.,<sup>26</sup> who used PEO–PS block copolymers with total molecular weight between 14 300 and 24 000 and PEO content between 7% and 24%. They have been shown that PEO–PS copolymers ( $M_w = 17\,136$  with wt PEO = 24% and  $M_w = 27\,332$  with wt PEO = 18%) formed monolayer films with hexagonal ordered dotlike morphology. In contrast, a PEO–PS copolymer ( $M_w = 14\,320$ ) with lower PEO content (9.2%) formed rodlike aggregates and another block copolymer with even lower PEO content ( $M_w = 23,988$ , wt PEO =

6.8%) displayed spaghetti-like surface morphology as was confirmed by TEM and AFM studies. In another paper, Cox et al.<sup>24</sup> demonstrated that a PEO-PS copolymer with higher PEO content ( $M_w = 18\ 080$  and wt PEO = 20%) showed hexagonal ordered dotlike morphology, which was reorganized at surface pressure around 6 mN/m. Three different models were discussed for block copolymer arrangement on the solid substrate. It has been confirmed that most likely the PS core sits on the top of a coherent PEO film, which protects the PS block from direct contact with the water surface. This agrees with Richards et al.<sup>29</sup> that the brush model for PS-PEO block copolymers deposited onto a solid substrate is unlikely.

Therefore, except in the case of PEO-PS block copolymer with extremely high molecular weight of both blocks, all credible studies for linear PEO-PS block copolymers with modest molecular weights (below 50 000) and low content of the PEO phase (below 24%) have shown that they are capable of forming a variety of surface morphologies as controlled by deposition conditions even for low surface pressures. In contrast, the surface behavior is very different for the asymmetric PEO-PS star block copolymers studied here where both architecture and chemical composition heavily favor the formation of highly curved interfaces. For the range of molecular weights studied here ( $M_n = 19\ 000$ – $47\ 000$ ) and PEO content (11–26%), star block copolymers formed stable circular morphology, which was preserved to high surface pressures with signs of circular-cylindrical transformation only observed for the highest pressures in star block copolymer with two PS arms. Increasing the number of PS arms to three stabilized the circular morphology of the monolayer while compression up to the pressures in the vicinity of the monolayer collapse. This trend can be associated with crowding state of the PS chains tethered to a single joint point as well as with a thermodynamically more stable curved shape of the interface in asymmetrical star-block copolymer as compared to a similar linear block copolymer.

**Acknowledgment.** Funding from Imperial Chemical Industries, SRF 2112 Contract and the National Science Foundation, DMR-0074241 grant is gratefully acknowledged. The authors thank V. V. Shevchenko, M. Ornatska, K. L. Genson, and B. Rybak for technical assistance.

## References and Notes

- (1) (a) Hsieh, H. L.; Quirk, R. P. *Anionic Polymerization: Principles and Practical Applications*; Marcel Dekker: New York, 1996. (b) *Star and Hyperbranched Polymer*; Mishra, M. K., Kobayashi, S., Eds.; Marcel Dekker: New York, 1999. (c) Sperling, L. H. *Introduction to Physical Polymer Science*, 3rd ed.; Wiley-Interscience: New York, 2001. (d) Hadjichristidis, N. *J. Polym. Sci., Part A. Polym. Chem.* **1999**, *37*, 857. (e) Matyjaszewski, K.; Xia, J. *Chem. Rev.* **2001**, *101*, 2921.
- (2) (a) Halperin, A.; Tirrell, M.; Lodge, T. P. *Adv. Polym. Sci.* **1992**, *100*, 33. (b) Zhao, B.; Brittain, W. J. *Prog. Polym. Sci.* **2000**, *25*, 677. (c) Koutos, V.; Van der Vegte, E. W.; Hadziioannou, G. *Macromolecules* **1999**, *32*, 1233. (d) Tsukruk, V. V.; Sidorenko, A.; Gorbunov, V. V.; Chizhik, S. A. *Langmuir* **2001**, *17*, 6715. (e) Tsukruk, V. V. *Adv. Mater.* **2001**, *13*, 95. (f) Julthongpiput, D.; Lin, Y.-H.; Teng, J.; Zubarev, E. R.; Tsukruk, V. V. *J. Am. Chem. Soc.* **2003**, *125*, 15912. (g) Green, P. F.; Christensen, T. M.; Russell, T. P.; Jerome, R. *Macromolecules* **1989**, *22*, 2(5), 2189.
- (3) Yang, L.; Hong, S.; Gido, S. P.; Velis, G.; Hadjichristidis, N. *Macromolecules* **2001**, *34*, 9069.
- (4) Zhu, L.; Huang, P.; Chen, W. Y.; Ge, Q.; Quirk, R. P.; Cheng, S. Z. D.; Thomas, E. L.; Lotz, B.; Hsiao, B. S.; Yeh, F.; Liu, L. *Macromolecules* **2002**, *35*, 3553.
- (5) Shen, J.; Zhang, X.; Yin, R. *Macromol. Chem. Macromol. Symp.* **1991**, *46*, 157.
- (6) Jeong, U.; Ryu, D. Y.; Kho, D. H.; Lee, D. H.; Kim, J. K.; Russell, T. P. *Macromolecules* **2003**, *36*, 4125.
- (7) Pispas, S.; Hadjichristidis, N.; Potemkin, I.; Khokhlov, A. *Macromolecules* **2000**, *33*, 1741.
- (8) Pispas, S.; Poulos, Y.; Hadjichristidis, N. *Macromolecules* **1998**, *31*, 4177.
- (9) Nakano, M.; Deguchi, M.; Endo, H.; Matsumoto, K.; Matsuoka, H.; Yamaoka, H. *Macromolecules* **1999**, *32*, 6088.
- (10) Mahltig, B.; Jérôme, R.; Stamm, M. *Phys. Chem. Chem. Phys.* **2001**, *3*, 4371.
- (11) Anastasiadis, S. H.; Retsos, H.; Pispas, S.; Hadjichristidis, N.; Neophytides, S. *Macromolecules* **2003**, *36*, 1994.
- (12) Mortensen, K.; Brown, W.; Almdal, K.; Alami, E.; Jada, A. *Langmuir* **1997**, *13*, 3635.
- (13) Zhu, L.; Chen, Y.; Zhang, A.; Calhoun, B. H.; Chun, M.; Quirk, R. P.; Cheng, S. Z. D.; Hsiao, B. S.; Yeh, F.; Hashimoto, T. *Phys. Rev. B* **1999**, *60*, 10022.
- (14) Zhu, L.; Cheng, S. Z. D.; Calhoun, B. H.; Ge, Q.; Quirk, R. P.; Thomas, E. L.; Hsiao, B. S.; Yeh, F.; Lotz, B. *Polymer* **2001**, *42*, 5829.
- (15) Reining, B.; Keul, H.; Höcker, H. *Polymer* **2002**, *43*, 7145.
- (16) Cogan, K. A.; Gast, A. P. *Macromolecules* **1990**, *23*, 745.
- (17) Hickl, P.; Ballauff, M.; Jada, A. *Macromolecules* **1996**, *29*, 4006.
- (18) Yu, K.; Eisenberg, A. *Macromolecules* **1996**, *29*, 6359.
- (19) Seo, Y.; Kim, M.; Ou-Yang, D.; Peiffer, D. *Polymer* **2002**, *43*, 5629.
- (20) Gonçalves da Silva, A. M.; Filipe, E. J. M.; d'Oliveira, J. M. R.; Martinho, J. M. G. *Langmuir* **1996**, *12*, 6547.
- (21) Pagac, E. S.; Prieve, D. C.; Solomentsev, Y.; Tilton, R. D. *Langmuir* **1997**, *13*, 2993.
- (22) Fauré, M. C.; Bassereau, P.; Carignano, M. A.; Szleifer, I.; Gallot, Y.; Andelman, E. *Phys. Lett. B* **1998**, *3*, 365.
- (23) Rother, G.; Findenegg, G. H. *Colloid Polym. Sci.* **1998**, *276*, 496.
- (24) Cox, J. K.; Yu, K.; Eisenberg, A.; Lennox, R. B. *Phys. Chem. Chem. Phys.* **1999**, *1*, 4417.
- (25) Faure, M. C.; Bassereau, P.; Lee, L. T.; Menelle, A.; Lheveder, C. *Macromolecules* **1999**, *32*, 8538.
- (26) Cox, J. K.; Yu, K.; Constantine, B.; Eisenberg, A.; Lennox, R. B. *Langmuir* **1999**, *15*, 7714.
- (27) (a) Baker, S. M.; Leach, K. A.; Devereaux, C. E.; Gragson, D. E. *Macromolecules* **2000**, *33*, 5432. (b) Devereaux, C. A.; Baker, S. M. *Macromolecules* **2002**, *35*, 1921.
- (28) Rivillon, S.; Munoz, M. G.; Monroy, F.; Ortega, F.; Rubio, R. G. *Macromolecules* **2003**, *36*, 4068.
- (29) (a) Richards, R. W.; Rochford, B. R.; Webster, J. R. P. *Polymer* **1997**, *38*, 1169. (b) Dewhurst, P. F.; Lovell, M. R.; Jones, J. L.; Richards, R. W.; Webster, J. R. P. *Macromolecules* **1998**, *31*, 7851.
- (30) Barentin, C.; Muller, P.; Joanny, J. F. *Macromolecules* **1998**, *31*, 2198.
- (31) Pitsikalis, M.; Pispas, S.; Mays, J. W.; Hadjichristidis, N. *Adv. Polym. Sci.* **1998**, *135*, 1.
- (32) Hawker, C. J. *Adv. Polym. Sci.* **1999**, *147*, 113.
- (33) Hadjichristidis, N.; Pispas, S.; Pitsikalis, M.; Iatrou, H.; Vlahos, C. *Adv. Polym. Sci.* **1999**, *142*, 71.
- (34) (a) Sheiko, S. S.; Möller, M. *Top. Curr. Chem.* **2001**, *212*, 137. (b) Ballauff, M. *Top. Curr. Chem.* **2001**, *212*, 177.
- (35) Xie, H.-Q.; Xie, D. *Prog. Polym. Sci.* **1999**, *24*, 275.
- (36) Tsitsilianis, C.; Papanagopoulos, D.; Lutz, P. *Polymer* **1995**, *36*, 3745.
- (37) Taton, D.; Cloutet, E.; Gnanou, Y. *Macromol. Chem. Phys.* **1998**, *199*, 2501.
- (38) Angot, S.; Taton, D.; Gnanou, Y. *Macromolecules* **2000**, *33*, 5418.
- (39) Francis, R.; Taton, D.; Logan, J. L.; Masse, P.; Gnanou, Y.; Duran, R. S. *Macromolecules* **2003**, *36*, 8253.
- (40) Gibanel, S.; Forcada, J.; Heroguez, V.; Schappacher, M.; Gnanou, Y. *Macromolecules* **2001**, *34*, 4451.
- (41) Heroguez, V.; Gnanou, Y.; Fontanille, M. *Macromolecules* **1997**, *30*, 4791.
- (42) Tsitsilianis, C.; Alexandridis, P.; Lindman, B. *Macromolecules* **2001**, *34*, 5979.
- (43) Francis, R.; Skolnik, A. M.; Carino, S. R.; Logan, J. L.; Underhill, R. S.; Angot, S.; Taton, D.; Gnanou, Y.; Duran, R. S. *Macromolecules* **2002**, *35*, 6483.

- (44) Kiriy, A.; Gorodyska, G.; Minko, S.; Stamm, M.; Tsitsilianis, C. *Macromolecules* **2003**, *36*, 8704.
- (45) (a) Tsukruk, V. V. *Prog. Polym. Sci.* **1997**, *22*, 247. (b) Luzinov, I.; Minko, S.; Tsukruk, V. V. *Prog. Polym. Sci.* **2004**, in press.
- (46) Falsafi, A.; Bates, F. S.; Tirrell, M. *Macromolecules* **2001**, *34*, 1323.
- (47) (a) Grubbs, R. B.; Dean, J. M.; Broz, M. E.; Bates, F. S. *Macromolecules*, **2000**, *33*, 9522. (b) Grubbs, R. B.; Broz, M. E.; Dean, J. M.; Bates, F. S. *Macromolecules*, **2000**, *33*, 2308.
- (48) Peleshanko, S.; Jeong, J.; Shevchenko, V., V.; Petrash, S.; Tsukruk, V. V. *Macromolecules* **2004**, submitted for publication.
- (49) Tsukruk, V. V.; Bliznyuk, V. N. *Langmuir* **1998**, *14*, 446.
- (50) (a) Azzam, R. M. A.; Bashara, N. M. *Ellipsometry and polarized light*, North-Holland Pub. Co.: New York, 1977. (b) Immergut, E. H.; Grulke, E. A. *Polymer Handbook*, John Wiley & Sons: New York, 1999.
- (51) Tsukruk, V. V. *Rubber Chem. Technol.* **1997**, *70*, 430.
- (52) Tsukruk, V. V.; Reneker, D. H. *Polymer*, **1995**, *36*, 1791.
- (53) Magonov, S. N.; Elings, V.; Whangbo, M.-H. *Surf. Sci.* **1997**, *375*, L385.
- (54) (a) Guzonas, D.; Boils, D.; Hair, M. L. *Macromolecules* **1991**, *24*, 3383. (b) Magonov, S. N. *Surface analysis with STM and AFM: experimental and theoretical aspects of image analysis*; VCH: Weinheim, Germany, and New York, 1996.
- (55) Israelachvili, J. N. *Intermolecular and surface forces*; Academic Press: San Diego, CA, 1991.
- (56) Alexander, S. *J. Phys.* **1977**, *38*, 983.
- (57) Small, D. M. *The Physical Chemistry of Lipids*; Plenum Press: New York, 1986.
- (58) Turner, C. M.; Sheller, N. B.; Foster, M. D.; Lee, B.; Corona-Glavan, S.; Quirk, R. P.; Annis, B.; Lin, J. S. *Macromolecules* **1998**, *31*, 4372.
- (59) (a) Grayer, V.; Dormidontova, E. E.; Hadziioannou, G.; Tsitsilianis, C. *Macromolecules* **2000**, *33*, 6330. (b) Zhu, Y.; Gido, S. P.; Moshakou, M.; Iatrou, H.; Hadjichristidis, N.; Park, S.; Chang, T. *Macromolecules* **2003**, *36*, 5719.
- (60) de Gennes, P. G.; Scalling, P. G. *Concepts in Polymer Physics*; Cornell University Press: Ithaca, NY, 1979.
- (61) Flory, P. J. *Statistical Mechanics of Chain Molecules*; Interscience Publisher: New York, 1969.
- (62) Aharoni, S. M. *Macromolecules* **1983**, *16*, 1722.
- (63) Wunderlich, B. *Macromolecular physics*; Academic Press: New York, 1973; Vol. 1.
- (64) Bailey, F. E., Jr.; Koleske, J. V. *Poly(Ethylene Oxide)*; Academic Press: New York, 1976.
- (65) Luzinov, I.; Julthongpipit, D.; Malz, H.; Pionteck, J.; Tsukruk, V. V. *Macromolecules* **2000**, *33*, 1043.
- (66) Shuler, R. L.; Zisman, W. A. *J. Phys. Chem.* **1970**, *74*, 1523.
- (67) (a) Ulman, A. *An Introduction to Ultrathin Organic Films: From Langmuir-Blodgett to Self-Assembly*; Academic Press: Boston, MA, 1991. (b) Spratte, K.; Riegler, H. *Makromol. Chem. Macromol. Symp.* **1991**, *46*, 113. (c) *Langmuir-Blodgett films*; Roberts, G.; Eds.; Plenum Press: New York, 1990. (d) Petty, M. *Langmuir-Blodgett films: an introduction*; Cambridge University Press: Cambridge, England, and New York, 1996.
- (68) Sheiko, S. S.; Prokhorova, S. A.; Beers, K. L.; Matyjaszewski, K.; Potemkin, I. I.; Khokhlov, A. R.; Moller, M. *Macromolecules* **2001**, *34*, 8354.
- (69) Lord, S. J.; Sheiko, S. S.; LaRue, I.; Lee, H.-I.; Matyjaszewski, K. *Macromolecules* **2004**, *37*, 4235.
- (70) (a) Tsukruk, V. V.; Bliznyuk, V. N.; Hazel, J.; Visser, D.; Everson, M. P. *Langmuir* **1996**, *12*, 4840. (b) Bliznyuk, V. N.; Everson, M. P.; Tsukruk, V. V. *J. Tribology* **1998**, *120*, 489.
- (71) Lee, M.; Kim, J.-W.; Peleshanko, S.; Larson, K.; Yoo, Y.-S.; Vaknin, D.; Markutsya, S.; Tsukruk, V. V. *J. Am. Chem. Soc.* **2002**, *124*, 9121.
- (72) Mazurina, E. A.; Myagkov, I. V.; Novak, V. R.; Belyaev, V. V. *Colloid J.* **2002**, *64*, 344.
- (73) Karim, A.; Tsukruk, V. V.; Douglas, J. F.; Satija, S. K.; Fetters, L. J.; Reneker, D. H.; Foster, M. D. *J. Phys., II* **1995**, *5*, 1441.
- (74) (a) Beyer, F. L.; Gido, S. P.; Uhrig, D.; Mays, J. W.; Tan, N. B.; Trevino, S. F. *J. Polym. Sci., Part B: Polym. Phys.* **1999**, *37*, 3392. (b) Mavrodios, A.; Avgeropoulos, A.; Hadjichristidis, N.; Thomas, E. L.; Lohse, D. J. *Chem. Mater.* **2003**, *15*, 1976.
- (75) Milner, S. T. *Macromolecules* **1994**, *27*, 2333.
- (76) (a) Pochan, D. J.; Gido, S. P.; Pispas, S.; Mays, J. W. *Macromolecules* **1996**, *29*, 5099. (b) Pochan, D. J.; Gido, S. P.; Pispas, S.; Mays, J. W.; Ryan, A. J.; Fairclough, J. P. A.; Hamley, I. W.; Terrill, N. J. *Macromolecules* **1996**, *29*, 5091.
- (77) Tsukruk, V. V.; Genson, K.; Peleshanko, S.; Markutsya, S.; Lee, M.; Yoo, Y.-S. *Langmuir* **2003**, *19*, 495.